NUMERICAL STUDY OF THE NEAR-FIELD OF HIGHLY UNDER-EXPANDED TURBULENT GAS JETS

Velikorodny A.[1]**, Kudriakov S.**[1]

[1] **CEA Saclay, DEN, DANS, DM2S/SFME,**
Gif-Sur-Yvette, France, e-mail : alexey.velikorodny@cea.fr

ABSTRACT

For safety issues related to the storage of hydrogen under high pressure, it is necessary to determine how the gas is released in the case of failure. In particular, there exist limited quantitative information on the near-field properties of the gas jets, which are important for establishing proper decay laws in the far-field. This paper reports recent CFD results for air and helium obtained in the near-field of the highly under-expanded jets. The gas jets are released from a 30-bar tank with the same opening (orifice). The Reynolds number based on the diameter of the orifice and corresponding gas conditions at the exit was well beyond 10^6. The 3D Compressible Multi-Component Navier-Stokes equations were solved directly without relying on the compressibility-corrected turbulence models. The numerical model was initially tested on a one-component (air-air) case, where a few aerospace-driven data sets are available for validation. The shock geometry is characterized through the Mach disk position and diameter. These are compared to the results known from the literature and to the scaling laws developed based on the dimensional analysis. In the second two-component (helium-air) jet scenario, the density field was validated and examined together with other fields, in the attempt to suggest potential initial conditions for the forthcoming far-field simulations.

1.0 INTRODUCTION

In aerospace and industrial applications, sonic and supersonic jets are often encountered. In particular, the accidental discharge of a high-pressure gas (e.g. hydrogen) into the atmosphere from a small opening in the vessel can result in under-expanded sonic/supesonic jet (pressure at the exit is much greater than atmospheric) until pressure in the vessel is sufficiently high. In these cases, knowledge of the temperature and flammable gas concentration are important in order to suggest the appropriate safety standards. However, there exist very limited quantitative information on the near-field properties of the gas jets, which are important for establishing proper decay laws in the far-field. Due to the great challenges that exist in measurements and calculations of the flow in the supersonic/subsonic shock-structured regions, in the literature currently there exist two simplifying approaches.

The first group of authors, including Birch et al. (1984) [1], [2], Yuceil and Otugen (2002) [3], among others, attempted to provide some correlations for velocity, temperature and/or concentration irrespective of the particulars in the initial expansion process of the underexpanded jet by using the notional nozzle concept. Initially, Birch et al. (1984) [1] developed this concept based on the ideal gas law, the equation of conservation of mass between the choked flow through the actual nozzle and a sonic flow through the notional nozzle. In addition, a uniform velocity profile and atmospheric temperature were assumed after jet expansion region. As underlined by Birch et al.

(1984) [1], the notional nozzle concept does not necessarily exist in the physical sense, and merely agrees with the chosen definition. Yuceil and Otugen (2002) [3], among others, attempted to advance the original concept by introducing the momentum and energy equations. This analysis provides the gas properties such as temperature and density at the notional location.

Despite this progress, there exist several reasons why application of the notional nozzle concept is in general questionable. In particular, it has been shown (e.g. Chenoweth (1983) [4]) that the ideal gas law overestimates the hydrogen/helium mass release by a significant amount for the very high pressure storage. The second problem rises from the assumption that there is no entrainment of the stationary fluid during the expansion and the initial species mass fraction remains unity. Therefore, another approach, alternative to the notional nozzle, was recently suggested by Xu et al. (2005) [5]. In this work axisymmetric Navier-Stokes equations with $k - \omega$ model were solved in the near-field of the highly under-expanded hydrogen jet (200-bar). Afterwards, the results of the computation including velocity, pressure, temperature and hydrogen mass fraction were analyzed to find the critical distance from the nozzle, where they considered to be most suitable for the subsequent Large Eddy Simulations (LES). However, the criteria, which provided this distance, was not clearly explained, as well as no attempt to validate the computation was performed. In addition, the results were averaged along the transverse coordinate to give the constant values of velocity, temperature, hydrogen mass fraction, etc.

Taking into account the outlined limitation of the previous study, it was attempted in this paper to solve 3D Compressible Multi-Component Navier-Stokes equations in the near-field of the highly under-expanded gas jets with the particular emphasis on the experimental validation of the numerical model. This allows a more physical description of the near-field properties of the gas jet and provision of the adequate initial conditions for the subsequent far-field simulations.

2.0 SHORT BACKGROUND

2.1 Shock-wave structure

The major parameter utilized to classify the various structures of the steady-state free under-expanded jet, discharging into the atmosphere is the pressure ratio $\frac{P_0}{P_\infty}$, where P_0 is the stagnation pressure in the tank and P_∞ is the ambient pressure. However, these shock-wave structures may also depend on the geometry of the nozzle and the nature of the gas, as it is discussed below. As the flow leaves the nozzle the high pressure mistmatch causes it to expand and accelerate. Expansion waves originate near the expansion point, propagate and meet the outer boundary of the jet, where they are reflected as compression waves. Coalescence of these waves results in a curved barrel shock surrounding the immediate supersonic region. For higher values of $\frac{P_0}{P_\infty}$ (> 15), which are considered herein, the shock structure is quite complex, as it is shown in Fig. 1 (from Wilke et al. (2008) [6]). The reflection of the incident shock is not regular anymore, and a so-called Mach disk pattern appears a few diameters downstream the orifice. The flow is subsonic just after the Mach disk, while it remains supersonic downstream of the barrel shock. The triple point connects various discontinuities and becomes the origin of a new slip line, which gives rise to a supersonic shear layer. The lengths of the shock cell and subsonic zone are increasing functions of pressure ratio and exit Mach number, while the diameter of the Mach disk is inversely proportinal to γ.

The most of the earlier experimental works, driven by the aerospace applications, were concentrated on the shock-wave structures, with particular emphasis on the location and size of the Mach disk (e.g. [7] - [12]). These studies established empirical correlations between the stagnation-to-ambient
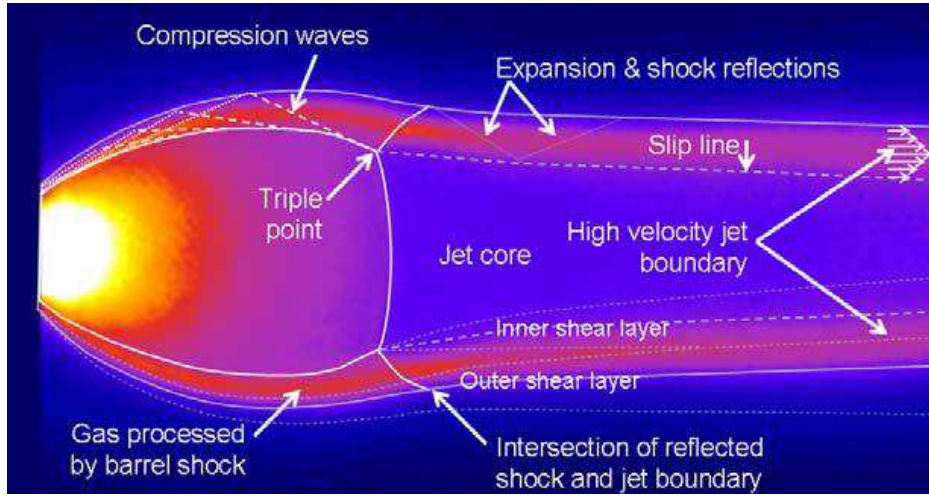
FIG. 1: Near-field of the highly underexpanded jet, [6]

pressure ratios and dimensions of the shock-wave structure for various gases. Discussion of these works is given in [13], however, it is worth mentioning that the Mach disk location, X_m, was shown to be very weakly dependant on γ by Ashkenas and Sherman (1966) [8] and on γ, stagnation temperature, condensation, nozzle lip geometry and absolute pressure level by Crist et al. (1965) [9]. Nevertheless, Bier and Schmidt (1961) [7] and [9] reported that the Mach disk diameter does significantly depend on the atomic nature of gas, condensation and γ, in particular. In view of this point, and in the context of the accidental discharge of high-pressure hydrogen (or helium), a theoretical analysis based on the dimensional groups was developed in [13] in order to predict the geometry of the shock-wave structure.

In short, it is apparent (e.g. [9]) that the size of the Mach disk for high pressure ratios substantially exceeds the diameter of the exit section. Thus, it is natural to consider the nozzle as the source and to characterize it by several quantities, including, the mass and momentum fluxes at the nozzle exit, and a maximum velocity during the discharge. Besides a diameter of the nozzle D_e, two more characteristic dimensions can be formed from the initial parameters. After some manipulations and for the special case of the sonic nozzle ($M_e = 1$), which might exist during the accidental release scenario, the dimensional groups can be reduced to

$$\frac{X_m}{D_e} = \frac{1}{2}\sqrt{\gamma}\sqrt{\frac{P_e}{P_\infty}} \times (\frac{\gamma + 1}{\gamma - 1})^{1/4} \tag{1}$$

$$\frac{D_m}{D_e} = kX_m\sqrt{1 - \frac{\gamma + 1}{\gamma} \times (\frac{\gamma + 1}{\gamma - 1})^{-1/2}} \tag{2}$$

where X_m and D_m are location and diameter of the Mach disk, P_e is the static pressure at the exit section, and k is an empirical constant, which accounts for the growth of the mixing layer and can not be predicted in this framework. The initial growth of the mixing layer (up to the location of the Mach disk) can be approximated using experimental measurements of Bier and Schmidt (1961) [7] given for various gases. It should be noted that these derivations are valid for the ideal gas law. However, at sufficiently high pressures the real gas state has to be utilized, as it was mentioned above. Therefore, although not used herein, the modifications of the present equations were also considered in [13] for the case of the high-pressure gas release.

2.2 Quantitative measurements and validation

Quantitative measurements in the near-field of the underexpanded jets are scarce due to the highly complex nature of the flow. In general, the physical probes could significantly alter the flow and thus are not well suited for these type of measurements. On the other hand the most of the early interesting experimental data in the near-field was obtained using impact techniques. For example, Glotov (1998) [14] utilized probes immediatly after the Mach disk to determine the length of the subsonic core (L_s). Correlation (3), thus obtained, can be used for $\frac{P_e}{P_\infty} <= 30$.

$$\frac{L_s}{D_m} = 1.96 \times (\frac{P_e}{P_\infty})^{-0.16} \tag{3}$$

The essentially non-intrusive methods such as laser Doppler velocimetry (LDV) and particle image velocimetry (PIV) show some promise for the quantitative characterization of supersonic jets. Chauveau et al. (2006) [15] performed extensive measurements of the hot under-expanded air jet with pressure ratios up to 40 and stagnation temperatures up to 2200 K with application to propulsion system exposed to engine fire. The results obtained were in satisfactory agreement with the in-house CFD predictions, which is encouraging in view of the complexity of the problem. The cold highly under-expanded air jets were studied recently by Yuceil et al. (2003) [16] for a range of stagnation-to-ambient pressure ratios (up to 38). Although, the choice of the experimental parameters, as well as experimental errors in this work, are open to questions, the centerline and transverse mean streamwise velocity profiles were found to be in good agreement between PIV, interferometric Rayleigh scattering (IRS) and Pitot pressure measurements. Similarly to previous works, the most dramatic particle intertia effect was found to be just downstream the Mach disk.

Later on, the planar laser-induced fluorescence (PLIF) was used in the experiments designed by Wilke et al. (2008) [6], targeting to simulate a leak through a hole in the surface of a hypersonic aerospace vehicle. Although, the PLIF images provide only qualitative spatial information about the jets structure (the fluorescence intensity depends on several local flow parameters, icluding pressure and temperature), certain useful properties of near-field can be acquired by looking at Fig.8 from [6]. It can be noted, that the upper and lower supersonic jet boundaries appear parallel many (> 40) diameters downstream. In addition, the shock and expansion reflections in these high-velocity boundaries (labeled in Fig.1) are visible.

Most recently, a large set of density/concentration measurements of the vertical turbulent subsonic and supersonic helium jets was performed by Dubois (2010) [17] using Background Oriented Schlieren (BOS) technique. The covered field up to 200 nozzle diameters and stagnation-to-ambient pressure ratios as large as 120 were considered. One of the particular findings of this work, which is in line with the results of Wilke (2008) [6], is that the potential core of the highly underexpanded jet is relatvely large compared to the ones ideally expanded. The empirical correlation provided by this study approximates the length of the potential core by $8 \times X_m$.

3.0 GOVERNING EQUATIONS AND NUMERICAL MODELING

3.1 Compressible Multi-Component Navier-Stokes equations

The viscous flow of a Newtonian multi-component fluid of N species is governed by the Navier-

Stokes equations which express the conservation of total mass (without source of mass), the mass conservation for species k ($k = 1, ..., N - 1$), conservation of momentum and energy [18],

$$\frac{\partial \rho}{\partial t} + \vec{\nabla} \cdot (\rho \vec{u}) = 0 \tag{4}$$

$$\frac{\partial \rho Y_k}{\partial t} + \vec{\nabla} \cdot \left(\rho (\vec{u} + \vec{V}_k) Y_k \right) = 0 \tag{5}$$

$$\frac{\partial \rho \vec{u}}{\partial t} + \vec{\nabla} \cdot (\rho \vec{u} \otimes \vec{u} + P\mathbf{I}) = \vec{\nabla} \cdot \underline{\underline{\tau}} + \rho \vec{g} \tag{6}$$

$$\frac{\partial \rho e_t}{\partial t} + \vec{\nabla} \cdot (\rho \vec{u} h_t) = \vec{\nabla} \cdot (\underline{\underline{\tau}} \cdot \vec{u} - \vec{q}) + \rho \vec{g} \cdot \vec{u} \tag{7}$$

The gas jet is considered to be either helium or air, with the pressure, temperature and density being coupled using the ideal gas law. The mass fractions Y_k, ($k = 1, ..., N$), the species density ρ_k and the mixture density are related by: $Y_k = \frac{\rho_k}{\rho}$ and Fick's law is used for the diffusion velocity $\vec{V}_k$ of species k

$$V_{k,i} Y_k = -D_k \frac{\partial Y_k}{\partial x_i} \tag{8}$$

with D_k being the diffusion coefficient of species k into the mixture. Following Stokes' hypothesis, the viscous shear stress tensor $\underline{\underline{\tau}}$ is given by:

$$\tau_{ij} = \mu \left(\frac{\partial u_i}{\partial x_j} + \frac{\partial u_j}{\partial x_i} - \frac{2}{3} \delta_{ij} \vec{\nabla} \cdot \vec{u} \right) \tag{9}$$

and the energy flux is

$$q_i = -\lambda \frac{\partial T}{\partial x_i} - \rho \sum_{k=1}^{N} h_k D_k \frac{\partial Y_k}{\partial x_i} \tag{10}$$

This flux includes a heat diffusion term expressed by Fourier's law and a second term associated with the diffusion of species with different enthalpies. The standard notations are used for the specific total energy, e_t, specific total enthalpy, h_t and specific internal enthalpy for the species k ($k = 1, ..., N$), h_k.

3.2 Numerical Discretisation and Turbulence Treatment

The system of equations (4)-(7) is solved using Finite Volume approach developed in the CAST3M code. The approximate Riemann-type methods are used for convective fluxes, which are either the van Leer splitting or the advection upstream splitting "AUSM+" methods. The "diamond"- type approach is employed for approximation of the diffusive fluxes. Overall, the scheme has a second order accuracy both in time and space.

Although a few simple eddy viscosity-type turbulence models are realized in CAST3M, an alternative approach is employed in view of the complexity of the problem, as well as thanks to the Finite Volume approach and monotonicity of the numerical schemes used. The present numerical model directly solves the governing equations without relying onto the subgrid-scale (SGS) turbulence models. Thus, the largerly controversial SGS models, especially those with compressibility-corrected terms, can be avoided. However, numerically generated viscosity inherent with numerical

algorithm has been shown to be rather effective turbulence model in many other investigations, including the work of Boris et al. (1992) [19], where the so-called MILES (Monotonically Integrated LES) approach has been introduced.

3.3 Computational domain and grid

As a starting point, the release from a relatively low pressure tank (30-bar) has been considered. The corresponding release velocities at the exit ($M_e = 1$) were 322 m/s and 892 m/s for air and helium, respectively. The flow field was initialized with air at 1 atm and a temperature of $300K$. The diameter of the opening (D_e) was fixed to be 0.01 m, which gives the Reynolds numbers well beyond 10^6 for both considered cases. The exit conditions were standart from the experimental point view, with the laminar velocity profile assumed at the inflow. All gas-dynamic parameters at the orifice, where the flow becomes choked, were calculated from the stagnation pressure and temperature using the ideal gas law (e.g. [20]).

In order to test the numerical model, including the size of the domain, boundary conditions, numerical schemes, etc., first, a relatively simple scenario of a one-component air-air jet release was considered. It is, however, clear that in the two-component helium-air case the scales and regimes of the flow can be substantially different. Therefore, the air-air release scenario is modeled using only quarter of the domain, in order to rapidly obtain the gross correlation with the available experimental results, while testing various parameters of the numerical model. In addition, this case permits to compare results with the axisymmetric simulations of Lehnasch (2005) [21], where so-called compressibility-corrected turbulence models were used.
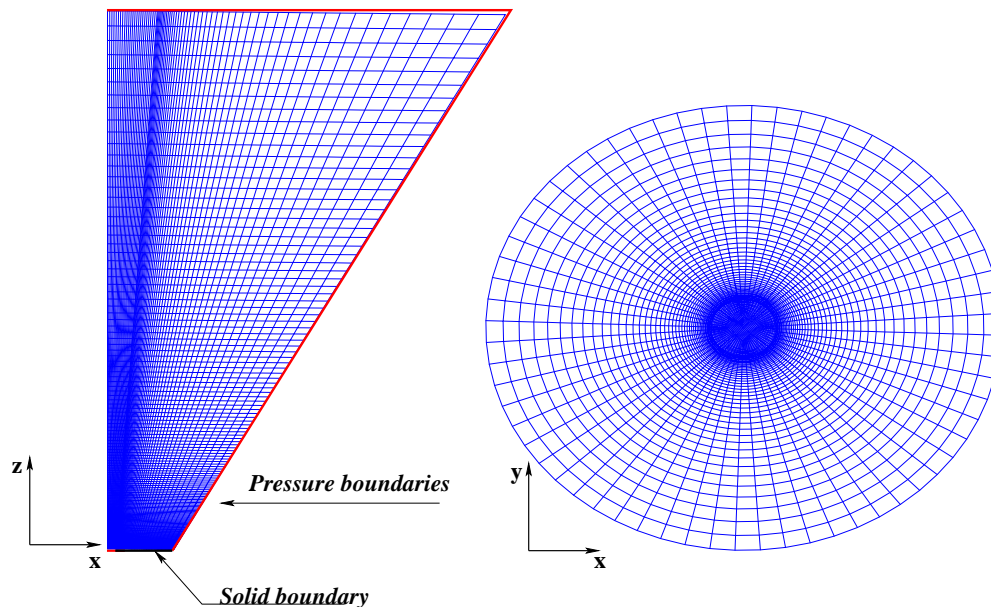

FIG. 2: Grid cross sections at y=0 and z=0. Red lines correspond to the inflow/outflow pressure boundaries, while the black one to the wall condition. Note: Only half of the vertical cut is shown.

A set of initial simulations (see Section 4.1) resulted in the computational domain, which has the following dimensions of the "base", vertical and "top" sections: $10D_e$, $35D_e$ and $48D_e$, respectively. As it is shown in Fig. 2 the no-slip boundary condition was set for the base, while the

pressure conditions (atmospheric) were prescribed at the outer boundaries to allow modelling of the entrainment. The latter was also improved by concentrating the computational volumes in the vicinity of the mixing region. The coarse (50x50x100) and fine (64x64x176) grids were used in the present work with the respective $X \times \theta \times Z$ resolution (with θ being an azimuthal coordinate). It should be noted, that a relatively coarse grid with under-resolution along Z-axis resulted in the non-physical shear layer emanating from the Mach disk in the proximity to the centerline for the air-air case. Thus, only fine grid case is shown for this scenario. The computations were performed until the flow reached a quasi-steady state with the time steps being approximately $2.5 * 10^{-8}$ and 10^{-8} for air and helium, respectively. In the course of this work it was found that the helium jet takes much more time to "stabilize". Because the helium-air case computations on the full domain are still in progress, only results computed with the quarter of the domain (using symmetry conditions) are shown herein. Nevertheless, the results are expected to be sufficiently accurate due to several specific features of the highly underexpanded jet, and its very large potential core length, in particular.

4.0 NUMERICAL RESULTS AND ANALYSIS

4.1 Simulations of the one-component (air-air) jet

It must be noted, that throughout this section, density, pressure and temperature are non-dimensionalized by their respective ambient values, while the magnitude of the exit velocity is used for the velocity field. In addition, following usual practice, time is made dimensionless as follows: $t^* = t\frac{U_e}{D_e}$.

Fig. 3 shows centerline values of axial streamwise velocity, Mach number, temperature and pressure. After exiting the orifice, the air jet undergoes great acceleration and cooling, which can be seen on the velocity and temperature plots. As a result the Mach number increases up to 5.36. This value is in good agreement with the semi-empirical formula given in [8]. It can be seen that the mean streamwise velocity increase behind the Mach disk correlates well both with the values measured using IRS by Yuceil et al. (2003) [16] and with the numerical simulations of Lehnasch (2005) [21]. However, the latter calculation overestimates the position of the Mach disk. The position X_m and diameter D_m of the Mach disk are compared in Table I to the values given in [21], obtained from the Schlieren visualization of [16], as well as with the early experimental correlations from various sources (see Section 2.1). Pressure in the proximity of the Mach disk drops quickly by about 2-orders of magnitude below its exit value. Beyond normal shock wave it increases sharply and rapidly returns to its ambient value. The temperature plot shows similar trends, however, temperature does not return to its field value throughout the domain. The maximum Mach number value of 0.89, which corresponds to the end of the subsonic core, is reached at $Z/D_e = 8.7$, while eqn. (3) predict the $X_m + L_s$ length to be $6.5D_e$. Lehnasch (2005) reports this distance to be about 3-times greater than the one given by correlations.

	Yuceil (Schl)	Present	Lehnasch	Correlations
X_m/D_e	3.6	3.73	3.86	3.56-3.67
D_m/D_e	1.85	1.88	2.14	1.82-2.23

TABLE I: Comparison of the position and diameter of the Mach disk (from various sources)

The transverse streamwise velocity profiles behind the Mach disk are shown in Fig. 4 at four downstream locations. In general, it is apparent that both simulations overestimate the peak
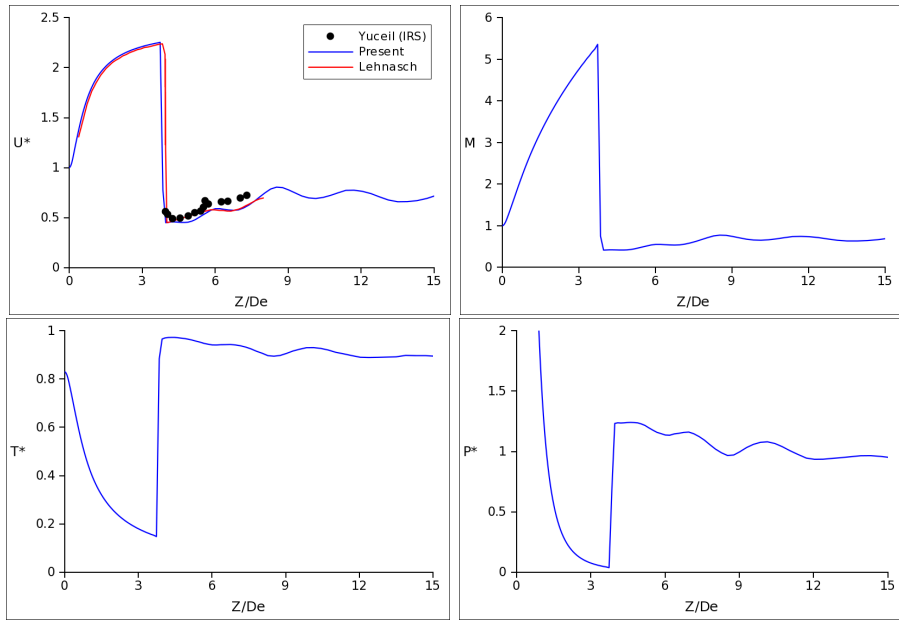
FIG. 3: Centerline values of streamwise velocity, Mach number, temperature and pressure
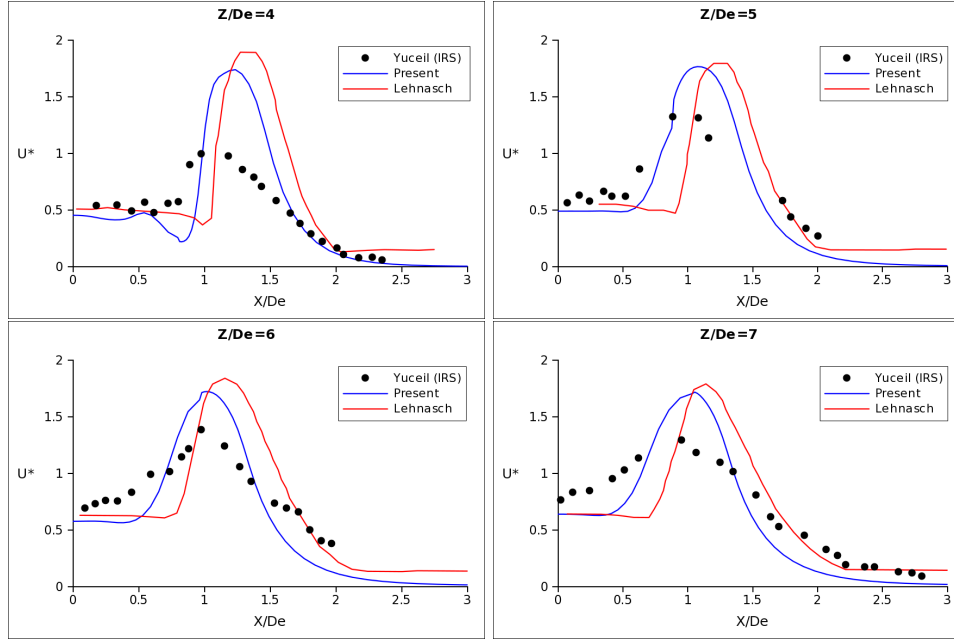

FIG. 4: Transverse velocity profiles behind the Mach disk at $Z = 4, 5, 6$ and $7D_e$, respectively

velocities of the jet, although, there are differences in particulars. The results of the present work provide fair predictions of the position of the maximum speed, which moves from about $X/D_e = 1.2$ to $X/D_e = 1$ with the downstream distance. Moreover, for $Z/D_e = 4$ and 5 the extent of the potential flow behind the Mach disk also compares relatively well. However, at $Z/D_e = 6$ as can be seen in the IRS data, the mixing layer generated at the triple point propagates through

the subsonic core, which is not well captured by the numerical model. It should be noticed, that Rayleigh scattering measurements in the supersonic regions may incur certain errors, especially due to the complicated calibration and high levels of noise.

4.2 Simulations of the two-component (helium-air) jet

The calculated position X_m and diameter D_m of the Mach disk are compared in Table II to the values obtained from the BOS visualizations of Dubois (2010) [17] and with the scaling laws shown in Section 2.1. Eqn. (2) appear to overestimate the diameter of the Mach disk, because the empirical constant k, as well as the assumption that the normal shock substantially exceeds dimensions of the exit section, work better for higher pressure ratios. It is, however, apparent that the computed ranges of the dimensions of the shock-wave structure are in general agreement with experiment. It was noted in Section 3.4 that the two-component gas jet took more time to reach quasi-steady state and, thus, the shock-wave structure take longer to develop. However, unstable behavior was observed even at later stages. The values of the Mach disk position and diameter corresponding to several time instants beyond $t^* > 90$ are shown in Table III.

	Dubois (BOS)	Present	Eqns. (1), (2)
X_m/D_e	3.5-3.8	3.6-4.1	3.58
D_m/D_e	1.25-1.75	1.54-1.8	2.09

TABLE II: Comparison of the position and diameter of the Mach disk with BOS and scaling laws

t^*	90	135	180	225	270	315	360
X_m/D_e	3.63	3.63	3.63	4.1	3.78	3.63	3.64
D_m/D_e	1.54	1.54	1.54	1.8	1.6	1.54	1.56

TABLE III: Position and diameter of the Mach disk in the present calculations as a function of non-dimensional time

The Mach number contours corresponding to the $t^* = 270$ and 225 are shown in Fig. 5 in order to demonstrate that the shock-wave structure was indeed time-dependent (at least initially) . It can be seen, that the thickness of the shear layer prior to the triple point changes with time together with the position and diameter of the Mach disk, as well as curvature of the barrel shock. Convective instabilities appear to be generated around the triple point and to propagate and grow in the supersonic region along the boundary of the potential core. The compressions and subsequent rarefactions, potentially produced by these vortex structures, are manifested in the oscillations of the supersonic shear layer along the potential core, which can be seen in the top image. Moreover, these pulsations are as well observed in the pressure plot of Fig. 6 below. It should be noted, that unsteady behavior of the supersonic gas jets has been observed in context of the aerodynamic jet noise. In addition, and being more close to the objectives of the present paper, Peneau et al. (2009) [22] have been reported the position of the Mach disk to vary significantly during the release of hydrogen from a high-pressure tank $(100atm)$ up to the $t^* = 80$ (corresponds to the end of the simulation).

Fig. 6 shows centerline values of the gas jet velocity, Mach number, density and pressure calculated using both coarse and fine grids. It can be seen, for the case of fine mesh, that all properties of
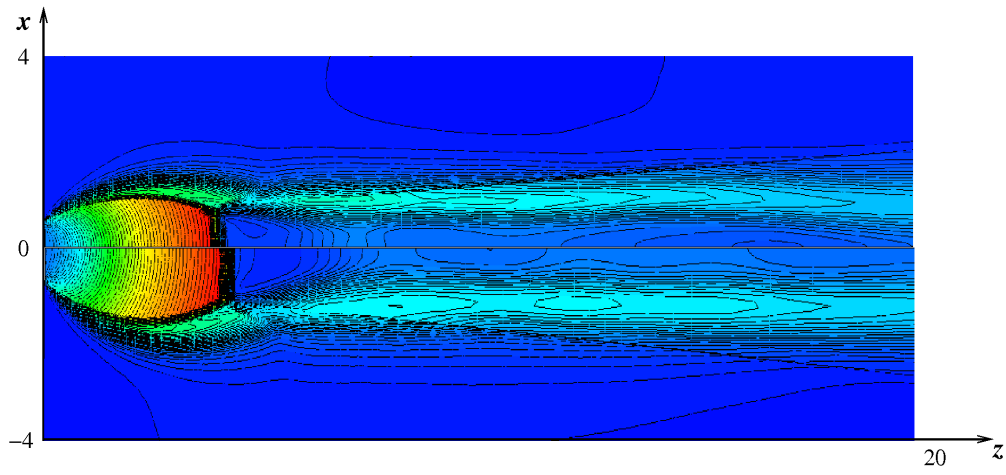
FIG. 5: Mach number contours at $t^* = 270$: top image, $t^* = 225$: bottom image; x and z coordinates are non-dimensionalized by D_e
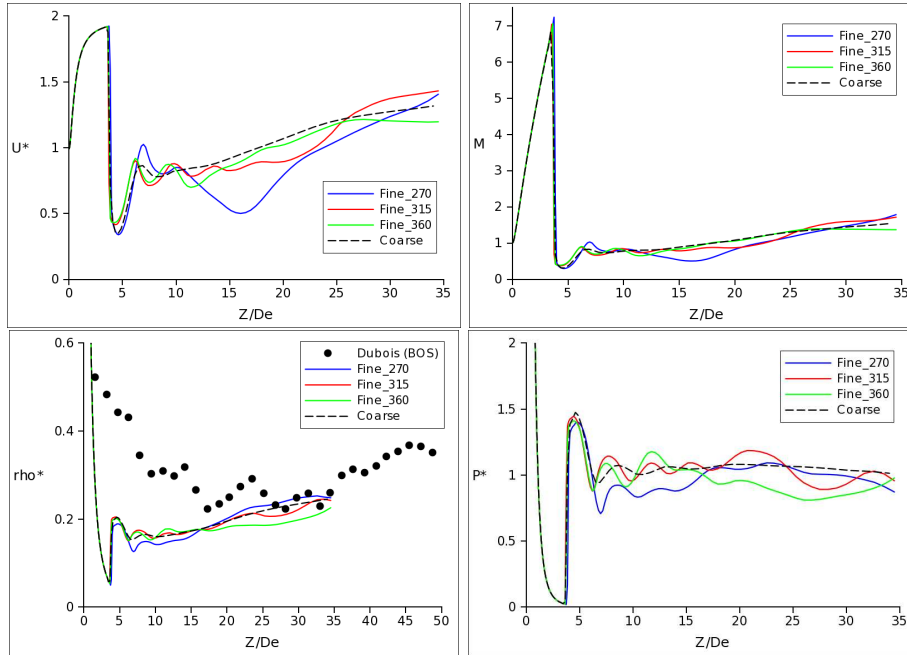

FIG. 6: Centerline values of streamwise velocity, Mach number, density and pressure

the helium gas jet at the centerline change substantially with time. However, on the coarse grid the solution converged much faster, and the results shown in Fig. 6, are in reasonable agreement with the data at $t^* = 360$ for fine mesh. The simulations are continued beyond that time and seem to confirm that a quasi-steady state solution was obtained. From the point of view of validation, the Mach number is observed to reach unity at $Z = 6.2$ for $t^* = 360$, which is in good agreement with the value of $6.5 D_e$ (with X_m being added) predicted by eqn. (3). According to the velocity plot ($t^* = 360$) the end of the potential core seems to be reached at $Z = 27 D_e$. In fact, this is in

agreement with measurements of [17], where the length of the potential core is approximated to be $8 \times X_m$ or about $29D_e$. The density measurements performed using BOS can not be compared in the regions, where temperature and pressure significantly different from the ambient. However, starting at about $17D_e$ the computations can be satisfactory validated by the experiments.
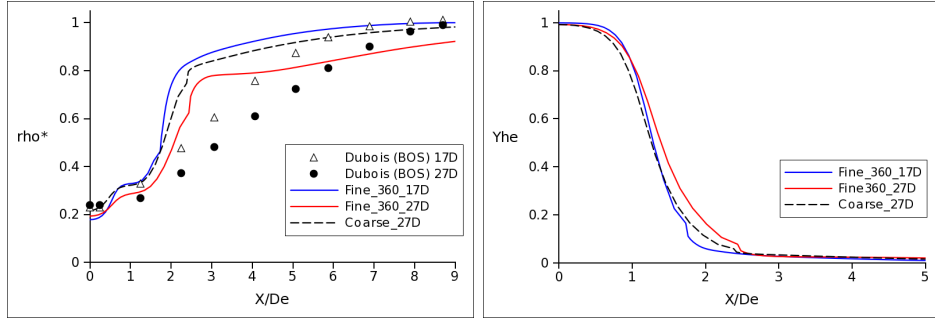

FIG. 7: Transverse profiles of density and helium mass fraction at $Z = 7$ and $17D_e$, respectively

In addition, transverse density and helium mass fraction profiles at $Z = 17D_e$ and $27D_e$ are plotted for fine and coarse grids. The computations performed using fine mesh overestimate jet density in the intermediate region from about $1.5D_e$ to $5D_e$. This can be attributed to the insufficient turbulent mixing provided by the low number of elements in this zone and may result in the underestimate of the helium mass fraction at the periphery of the jet. On the other hand the transverse BOS data might suffer from the non-ambient temperature effects, which could exist in this region. It can be also seen, that density profile calculated using coarse grid shows greater error compared to the experimental data at $Z = 27D_e$. This is expected, in view of the turbulence treatment methodology (see Section 3.2) used in the present study.

5.0 CONCLUSIONS

Simulations of the highly under-expanded turbulent gas jets were performed and compared with the available experimental data sets and correlations. The numerical model provides relatively fair mean predictions both in the case of the one-component air-air and two-component helium-air scenarios. In particular, the position and diameter of the Mach disk, and especially the length of the subsonic core behind the Mach disk were found to be in good agreement with experimental measurements. However, the density profiles have shown substantial difference compared to the BOS results in the regions of relatively coarse mesh (at the periphery of the jet).

Unsteady behaviour of the helium gas jet have been observed after a few flow through times. At this point, the simulations are in progress, and the transient data is being gathered, in order to provide more information on the nature of instability involved in this flow regime. In addition, the acquired quantitative data can be used as fluctuating (periodic) initial conditions for the forthcoming far-field simulations.

ACKNOWLEDGMENTS

REFERENCES

[1] Birch, A.D., Brown, D.R., Dodson, M.G., Swaffield, F., The structure and concetration decay of high pressure jets of natural gas, *Combustion science and Technology*, 36, 1984, pp. 249-261.

[2] Birch, A.D., Huches, D.J., Swaffield, F., Velocity Decay of High Pressure jets, *Combustion science and Technology*, 52, 1987, pp. 161-171.

[3] Yuceil, K.B., Otugen, M.V., Scaling parameters for underexpanded supersonic jets, *Physics of Fluids*, 14-12, December 2002, pp. 4206-4215.

[4] Chenoweth, D.R., Gas-transfer analysis section H-real gas results via the van der Waals equation of state and virial expansion extensions of its limiting Abel-Noble form, *Sandia report*, SAND83-8229, June 1983.

[5] Xu, B.P., Zhang, J.P., Wen, J.X., Dembele, S., Karwatzki, J., Numerical study of a highly underexpanded hydrogen jet, International Conference on Hydrogen Safety, Pisa, Italy, 8-10 September 2005.

[6] Wilke, J.A., Danehy, P.M., Nowak, R.J., Alberfert, D.W., Fluorescence Imaging Study of Impinging Underexpanded Jets, 46th AIAA Aerospace Sciences Meeting and Exhibit, Reno, NV, 7-10 January 2008.

[7] Bier, K., Shcmidt, B., Zur Form der Verdichtungsstibe in frei expandierenden Gasstrahlen, *Z.f.angew. Physik*, 13, 1961 pp. 493-500.

[8] Ashkenas, H., Sherman, F.S., Structure and utilization of supersonic free jets in low density wind tunnels, *Rarefied Gas Dyn.*, 2, 1966, pp. 84-105.

[9] Crist, S., Sherman, P.M., Glass, D.R., Study of the highly underexpanded sonic jet, *AIAA Journal*, 4-1, 1965, pp. 68-71.

[10] Love, E.S., Grigsby, C.E., Lee, L.P., Woodling M.J., Experimental and theoretical studies of axisymmetric free jets, *NASA Technical report*, R-6, 1959, pp. 1-292.

[11] Avduevskii, V.S., Ivanov, A.V., Karpman, I.M., Traskovskii V.D., Yudelovich, M.Ya., Flow in supersonic viscous underexpanded jet, *Translated, Izv. Akad. Nauk SSSR, Mekhanika Zhidkosti i Gaza*, 5-3, Sept 1970, pp. 409-414.

[12] Addy, A.L., Effects of axisymmetric sonic nozzle geometry on Mach disk characteristics jets, *AIAA Journal*, 19, Jan 1981, pp. 121-122.

[13] Velikorodny, A., Overview of highly underexpanded jets: application to the accidental release of gas from a high-pressure reservoir, *Rapport DEN/DANS*, SFME/LTMF/RT/10-016/A, January 2011.

[14] Glotov, G.F., Local subsonic zones in supersonic jets flows, *Fluid Dynamics*, 33-1, 1998, pp. 117-123.

[15] Chauveau, C., Davidenko, D.M., Sarh, B., Gökalp, I., Avrashkov, V., Fabre, C., PIV Measurements in an Underexpanded Hot Free Jet, 10th International Symposium on Application of Laser Techniques to Fluid Mechanics, Lisbon, Portugal, 26-29 June 2006.

[16] Yuceil, K.B., Otugen, M.V., Aric, E., Interferometric Rayleigh scattering and PIV measuremnts in the near-field of underexpanded sonic jets, 41st Aerospace Sciences Meeting and Exhibit, Reno, Nevada, 6-9 January 2003.

[17] Dubois, J., Étude expérimentale de jets libres, compressibles ou en présence d'un obstacle, *PhD thèse*, Aix Marseille Université, June 2010.

[18] Poinsot, T., Veynante, D., Theoretical and Numerical Combustion, *Edwards*, (2001)

[19] Boris J.P., Grinstein F.F., Oran E.S., Kolbe R.J., New Insights into Large Eddy Simulation, *Fluid Dynamic Research*, 1992.

[20] Landau, L.D., Lifshitz, E.M. Fluid Mechanics (Course of Theoretical Physics), *Pergamon Press*, 2-nd edition, July 1987.

[21] Lehnasch, G., Contribution à L'étude numérique des jets supersoniques sous-dètendus, *PhD Thèse*, L'Université de Poitiers, 2005.

[22] Peneau, F., Pedro, G., Oshkai, P., Djilali, N., Transient supersonic release of hydrogen from a high pressure vessel: A computational analysis, *Journal of Hydrogen Energy*, 34-14, 2009, pp. 5817-5827.